Intrinsic features of the magnetoeletric coupling mechanism in displacive multiferroics

V. F. Freitas, D. Z. Montanher, T. G. M. Bonadio, V. L. Mazzocchi, J. Mestnik-Filho et al.

Citation: J. Appl. Phys. **114**, 134102 (2013); doi: 10.1063/1.4824283
View online: http://dx.doi.org/10.1063/1.4824283
View Table of Contents: http://jap.aip.org/resource/1/JAPIAU/v114/i13
Published by the AIP Publishing LLC.

JOURNAL OF APPLIED PHYSICS **114**, 134102 (2013)

Intrinsic features of the magnetoeletric coupling mechanism in displacive multiferroics

V. F. Freitas,[1] D. Z. Montanher,[1] T. G. M. Bonadio,[1] V. L. Mazzocchi,[2] J. Mestnik-Filho,[2] C. B. R. Parente,[2] D. Garcia,[3] J. A. Eiras,[3] L. F. Cótica,[1,4] and I. A. Santos[1]
[1]*Department of Physics, State University of Maringá, Maringá, Paraná 87020-900, Brazil*
[2]*Instituto de Pesquisas Energéticas e Nucleares (IPEN-CNEN/SP), São Paulo, São Paulo CP 11049, Brazil*
[3]*Department of Physics, Federal University of São Carlos, São Carlos, São Paulo 13565-905, Brazil*
[4]*Department of Electrical and Computer Engineering, University of Texas, San Antonio, Texas 78249, USA*

(Received 22 July 2013; accepted 18 September 2013; published online 2 October 2013)

Structural, ferroelectric, and magnetic arrangements, and electron density in the vicinity of cations, were modeled from high-resolution X-ray and neutron powder diffraction data in La modified $BiFeO_3$-$PbTiO_3$ compounds. Important features for controlling the intrinsic mechanism for the magnetoelectric coupling in these materials, as prototypes for perovskite structured magnetoelectric multiferroics, are pointed out and discussed. It is shown that the magnetoelectric coupling angle is governed by covalent-like forces, which also affect the structural and ferroelectric distortions in the unit cell. © *2013 AIP Publishing LLC*. [http://dx.doi.org/10.1063/1.4824283]

I. INTRODUCTION

The framework of structural, electric, and magnetic properties of multiferroic magnetoelectrics aiming at multifunctional applications has been studied for several decades.[1,2] In fact, many potentially advanced technological devices based on multiferroic magnetoelectric materials, such as magnetically tunable electromechanical transducers and magnetoelectric high-power solid state transformers, depend on the macroscopic magnetic response of these materials.[3,4] Alternative routes such as site-specific cationic modifications have been suggested to increase the resulting magnetization.[5,6] Perovskite structured (ABO_3 type) $BiFeO_3$ (BF) and BF-based $(Bi(Mn,Fe)O_3$, $(Bi,La)FeO_3$, $BiFeO_3$-$BaTiO_3$ and $BiFeO_3$-$PbTiO_3$, etc.,) compounds, for instance, show ferroelectric, (weak/anti)ferromagnetic orders and magnetoelectric coupling at room temperature. Moreover, these materials seem to be among the few compounds with potential for practical multiferroic applications.[7] Due to their rhombohedral symmetry, an energetically favorable weak canting of the anti-parallel spins carries a resultant magnetic moment (a weak-ferromagnetic arrangement), as predicted by the Dzialoshinski-Morya theory.[8,9] Interestingly, from the magnetic point of view, B-site modified BF-based systems can be considered as a magnetic dilution of the BF compound.

In such context, La-doped $BiFeO_3$-$PbTiO_3$ (BFPT-L) solid solutions emerge as favorite candidates for practical applications among the few proposed in literature.[10,11] These compounds show the characteristics which, according to Hill,[12] allow for the occurrence of magnetoelectric coupling at room temperature. Among them, BFPT-L solid solutions crystallize in 3*m*, 3*c*, or 4*mm* point groups show high electrical resistivity, weak-ferromagnetism, or antiferromagnetism (completely tuned by the addition of La),[13] and specially hybridized A-O and B-O chemical bonds,[14] which allow for the distortions of the d^n electronic sublayer, thus inducing the magnetoelectric coupling.[15] Furthermore, in BFPT-L compounds some magnetic ions (Fe^{3+}) are replaced by non-magnetic ones (Ti^{4+}), and the magnetic spiral structure of the BF matrix is indeed broken, releasing the macroscopic spontaneous magnetization.[3]

From the structural point of view, the BF matrix changes from a rhombohedral (*R*3*c* space group) to a tetragonal (*P*4*mm* space group) symmetry with the increase of PT concentration in BFPT solid solutions. This structural evolution leads to the coexistence of dissimilar symmetric phases (*R*3*c* and *P*4*mm*), at ~30% of PT, characterizing a morphotropic phase boundary (MPB).[16,17] Interestingly, another structural change occurs with the addition of La into BFPT. As an example, the tetragonal $(0.6)BiFeO_3$-$(0.4)PbTiO_3$ compound undertakes a rhombohedral symmetry (>5 wt. % of La), also passing through an MPB region (at ~3 wt. % of La).[13] It is worth noting that a rigorous study on the intrinsic mechanisms that link ferroic orders (ferroelectric and magnetic) and the structural features that govern the magnetoelectric coupling is highly desirable for the understanding of how the BFPT-5L compound, as well as other displacive multiferroics would be used in technological applications. This study analyses the intrinsic link between ferroism and atomic structure in the BFPT-5L compound, as a prototype for BF-based perovskites, through high-resolution neutron powder (HR-NPD) and high-resolution X-ray powder (HR-XPD) diffraction experiments combined with structural refinement (Rietveld). A complex magnetic structure is proposed by using irreducible representations, and the spatial configuration of electric and magnetic moments is exposed by superposing magnetic and atomic structures. Consequently, the intrinsic physical mechanism that leads to the magnetoelectric coupling in these compounds is revealed.

II. EXPERIMENTAL

Stoichiometric $(0.6)BiFeO_3$-$(0.4)PbTiO_3 + 5$ wt. % La_2O_3 (BFPT-5L) polycrystalline samples were synthesized as previously reported.[11,18] HR-NPD data ($\lambda_N = 1.4119$ Å, $2\theta = 10°$ to 110°, and T = 300 K) were collected at AURORA, the high-resolution powder diffractometer installed at the IEA-R1 research reactor of the Instituto de

Pesquisas Energéticas e Nucleares (IPEN-CNEN/SP), São Paulo, SP, Brazil.[19] Synchrotron HR-XPD measurements were performed on the diffractometer installed at the XPD experimental station of the Brazilian Synchrotron Light Laboratory (LNLS), Campinas, SP, Brazil ($\lambda_X = 1.549560$ Å, $2\theta = 10°$ to $110°$, T = 300 K). These data (from HR-NPD and HR-XPD measurements), carrying magnetic and structural information, were analyzed by the Rietveld method using the FullProf software.[20] The neutron diffraction data were best represented by a model consisting of a conventional structure (*R*3*c*), to describe nuclear scattering, and another purely magnetic structure (magnetic Fe^{3+} ions in a G-type antiferromagnetic order), to describe the magnetic scattering. The magnetic structure was described by a reversal operator **R** combined with a standard crystallographic operation (−*1*) at the triclinic symmetry (*P1*), in the so-called irreducible representation (IR).[21] The IR for the BFPT-5L sample was obtained by using the BasIReps software (FullProf package). The arrangement of magnetic moments was visualized with the FullProf studio (version 2.0) software, while the tree-dimensional structural viewing was constructed with the VESTA (*Visualization for Electronic and Structural Analysis*—3.0.7) software.[22,23] The polarization vector (magnitude and direction) was calculated from the atomic positions of cations and anions obtained by Rietveld refinement and then visualized by VESTA, associated with occupancy factor, atomic contribution, and ionic charge. Magnetic and magnetoelectric characterizations were performed at 300 K using a Lake Shore (7307-7 Inch) vibrating sample magnetometer and the dynamic magnetoelectric characterization set-up.[24]

III. RESULTS AND DISCUSSION

Figure 1 shows ferroelectric, magnetic, and magnetoelectric responses for the BFPT-5L sample at room temperature. The ferroelectric hysteresis curve (Fig. 1(a)) reveals a typical ferroelectric behavior ($P_r \sim 10\,\mu C/cm^2$, $P_s \sim 15\,\mu C/cm^2$, and $E_c \sim 22$ kV/cm). The BFPT-5L compound also shows a small magnetic response (Fig. 1(b)) typical of antiferromagnetic (AFM) samples with low remanence (as shown in the inset of Figure 1(b)) and unsaturated magnetization at the field strengths used in this work. However, continuous La addition in BFPT leads to high magnetic responses, as demonstrated in previous works.[13,14] The magnetoelectric response was also determined and the magnetoelectric coefficient α_{33}, shown in Fig. 1(c), reached elevated values ($\alpha_{33} \sim 3.55$ mV/cm · Oe) in comparison with the typical values ($\alpha_{33} \sim 0.88$ mV/cm · Oe) assessed for BFPT samples with high La concentrations (~50% of La).[15] As mentioned, these results indicate the considerable potential of the BFPT-5L compound for practical applications in which the magnetoelectric effect is required, as in multiple state non-volatile memory devices.[25,26]

Figure 2 shows HR-NPD and HR-XPD patterns for the BFPT-5L sample at room temperature. The ND patterns revealed a purely magnetic reflection labeled M(111) among other reflections that are superimposed patterns of magnetic and chemical (nuclear) structures (see Fig. 2(a)). The

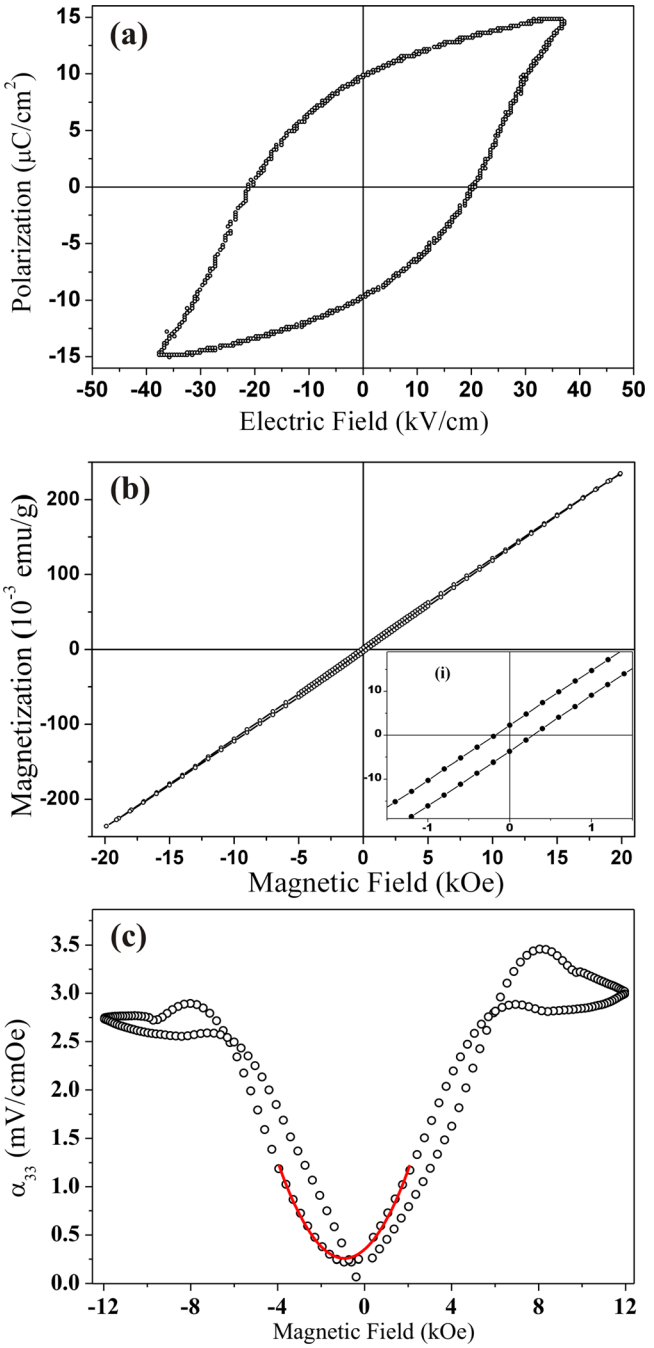

FIG. 1. Ferroic properties for the $(0.6)BiFeO_3$-$(0.4)PbTiO_3$ + 5 wt. % La compound at room temperature. (a) Ferroelectric (at 30 Hz) and (b) magnetic hysteresis curves. (c) Magnetoelectric coefficient as a function of the magnetic field (at 1 kHz and 6 Oe (rms)). Red (online) or black solid line—quadratic fit. (i) Enlarged view of the low magnetic field region.

structural model that fully describes the BFPT-5L compound is similar to that of the BF compound, i.e., a single perovskite structure with a *R*3*c* space group in a rhombohedral symmetry.[27,28] A comparative analysis between the Rietveld refined parameters of HR-NPD and HR-XPD (Table I) gives rise to consistent structural parameters (lattice parameters and atomic positions) and reliability factors (R_B, R_F, R_M, and χ).[29] Some slightly disperse values between the HR-NPD and the HR-XPD refined data appeared due to the fact that the oxygen ions show a smaller X-ray scattering power than neutrons.

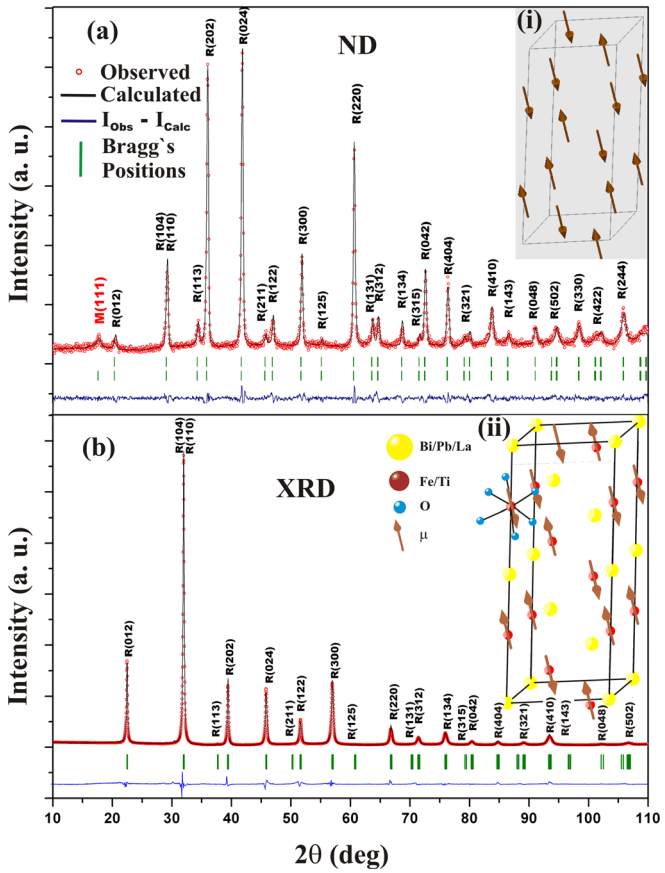

FIG. 2. Rietveld refinement results of (a) high-resolution neutron and (b) high-resolution X-ray powder diffraction data for the $(0.6)BiFeO_3$-$(0.4)PbTiO_3 + 5$ wt. % La compound, at room temperature. Insets: (i) Magnetic structure in the hexagonal representation. (ii) Superimposed magnetic and structural lattices in the hexagonal representation.

The best fit for HR-NPD data was achieved with a magnetic model (along with the crystallographic structural model) consisting of a G-type antiferromagnetic order, which forms a magnetic pseudo-cubic structure with magnetic moments ferromagnetically ordered within the $(111)_R$ plane, and antiferromagnetically ordered relatively to the adjacent plane (see Fig. 3(a)—red (online) or light gray plane). The AFM ordering is achieved through the indirect superexchange interactions that occur between magnetic ions (Fe^{3+} ions mediated by oxygen).[30–32] The proposed magnetic model was composed by a reversal operator (**R**), combined with an inversion operator (-1) in the triclinic ($P1$) symmetry with $R3c$ atomic lattice parameters.[33,34] The magnetic moment was constrained to the *ac*-plane of the nuclear lattice in the hexagonal representation of the perovskite $R3c$ structure. Based on a previous report,[33] the Fe moment was set to 3.0 μ_B. Hence, the initial direction of the magnetic moment vector was preset to the 202_H direction. Commonly reported magnetic models for BF and BF-based compounds presume that the magnetic moments are perpendicular (within the *ab*-plane of the hexagonal representation)[33] or parallel (in the *c*-direction) to the direction of the electric dipole moment (polarization vector).[35] However, previous works[36] have indicated that the magnetoelectric coupling in $BiFeO_3$ tends to occur when the magnetic moments are enclosed in the rhombohedral plane that contains the magnetic cycloid (*ac*-plane of the hexagonal representation). In

TABLE I. Rietveld refinement results for the $(0.6)BiFeO_3$-$(0.4)PbTiO_3$ + 5 wt. % La sample. Lattice parameters for hexagonal (a_H, c_H) and rhombohedral (a_R, α_R) symmetries; atomic positions for the hexagonal symmetry ($Z_{Bi/Pb/La}$, $Z_{Fe/Ti}$, X_O, Y_O, and Z_O); magnetic moment by atom (μ_{Fe}/μ_B); polarization per unit cell (P); and reliability factors (R_B, R_F, R_M, and χ^2).

Parameter	Neutrons	X-rays
a_H (Å)	5.5910(2)	5.5990(1)
c_H(Å)	13.711(4)	13.732(4)
a_R (Å)	3.9550(1)	3.9608(2)
α_R (°)	89.95	89.95
$Z_{Bi/Pb/La}$	0.1257(1)	−0.0639(2)
$Z_{Fe/Ti}$	0.3893(8)	0.24042(3)
X_O	0.4639(5)	0.4895(1)
Y_O	−0.0085(7)	0.0257(9)
Z_O	1.1473(3)	0.9511(9)
μ_{Fe}/μ_B	4.18	—
P ($\mu C/cm^2$)	31.53(9)	—
R_B	3.71	4.53
R_F	2.78	5.07
R_M	8.43	—
χ^2	4.35	4.63

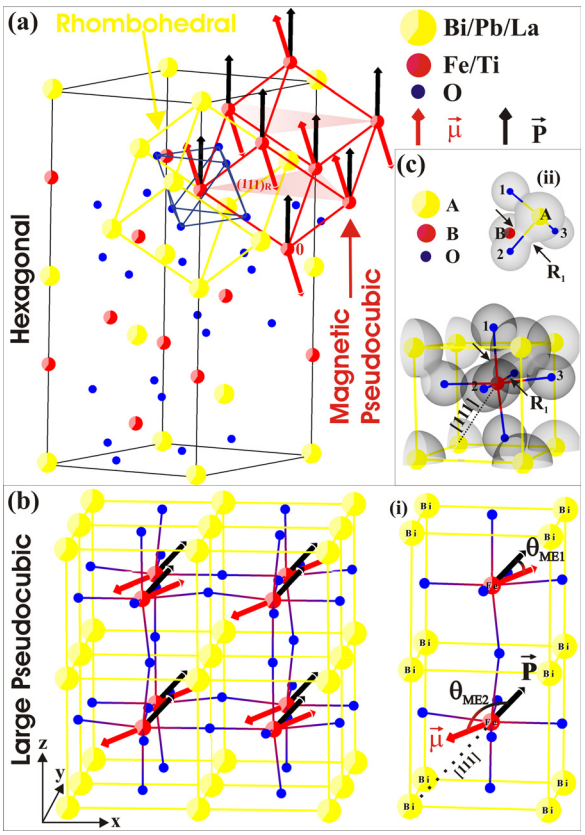

FIG. 3. Structural, antiferromagnetic, and ferroelectric mechanisms in $(0.6)BiFeO_3$-$(0.4)PbTiO_3 + 5$ wt. % La compound. (a) Magnetic ($P1$) red (online) or dark gray lines, nuclear ($R3c$) structures with hexagonal (black lines) and rhombohedral (yellow (online) or light gray lines) symmetries, (μ) magnetic (red (online) or dark gray arrows) and ($\vec{p}$) electric (black arrows) dipoles in the hexagonal cell; (b) large pseudocubic (overlapping of eight rhombohedral cells) symmetry with magnetic and electric dipoles (i) inset—Magnetoelectric angles (θ_{ME1} and θ_{ME2}) in the rhombohedral symmetry; (c) Modeled electron density (ii) inset—Highlighted chemical covalent bond.

fact, these authors have indicated that the magnetoelectric coupling energy reaches a maximum when the polarization direction occurs in the same plane of the magnetic cycloid (as in this case), and a minimum when it is perpendicular to that plane. Since the magnetic behavior of BFPT-5L originates from the BF matrix, it is possible to understand it likewise. That is, when the magnetic cycloid is broken in BFPT-5L by the insertion of Ti ions in the B site of the perovskite cell, the magnetic moments remain in the cycloid plane, thus facilitating the magnetoelectric coupling, as shown in Fig. 1(c). The proposed magnetic model is perfectly fitting to the experimental neutron diffraction data. However, given that the amount of experimental information about the magnetic structure is smaller than that of nuclear information, the obtained directions for magnetic moments carry a relative uncertainty.

By using this protocol, the resultant magnetic moment per Fe^{3+} ion ($\mu_{Fe} = 4.18(2)\ \mu_B$) obtained from the Rietveld refinement is consistent with the one reported for pure BF ($4\ \mu_B$),[37,38] La, and Mn doped BF ($3.75\ \mu_B$).[39,40] It is also consistent with those moments found for BFPT solid solutions with different compositions ((0.9)$BiFeO_3$-(0.1)$PbTiO_3$ ($3.83\ \mu_B$),[33] (0.8)$BiFeO_3$-(0.2)$PbTiO_3$ ($5.8\ \mu_B$),[35] and (0.7)$BiFeO_3$-(0.3)$PbTiO_3$ ($4.1\ \mu_B$)).[34] In fact, no significant changes in the magnetic moment per magnetic ion of BFPT-5L are expected from the comparison of this system with other pure or modified BF systems. The most significant change is expected to occur in the global (macroscopic) magnetization due to the breakdown of the long-range magnetic network.[3] The spatial representation of the magnetic moment vector ($\vec{\mu} = 2.948\hat{x} + 0.00\hat{y} + 0.2936\hat{z}$) is show in Fig. 2(a) (inset (i)—dark red (online) or black arrows inserted). The superimposition of $\vec{\mu}$ vectors (red (online) or light gray arrows) with the atomic structure is shown in the inset of Fig. 2(b)—inset (ii), revealing the crystallographic direction of the resultant magnetization in the BFPT-5L compound.

The complete structural description in the hexagonal and rhombohedral representations, containing the magnetic and ferroelectric moment vectors, as well as the angle between them in both representations, is shown in Fig. 3. The rhombohedral and magnetic pseudocubic representations were highlighted in the hexagonal cell to emphasize that these symmetries coexist in the BFPT system (Fig. 3(a)). Furthermore, the magnetic $\vec{\mu}$ and electric ($\vec{p} = 0.00\hat{x} + 0.00\hat{y} + 0.20\hat{z}$) dipole vectors (in hexagonal representation) are also highlighted in Fig. 3(a). Since the hexagonal representation is standard for the Rietveld refinement analysis protocol, the conversion from the hexagonal to the less complex rhombohedral-large pseudocubic symmetry is necessary to facilitate the analysis/visualization of the intrinsic magnetoelectric coupling mechanism. Thus, the position parameters of such large pseudocubic symmetry (Fig. 3(b)) can be obtained from the hexagonal parameters by the following conversion matrix:[41,42]

$$\begin{pmatrix} 2/3 & 2/3 & -4/3 \\ -2/3 & 4/3 & -2/3 \\ 1/3 & 1/3 & 1/3 \end{pmatrix}, \quad (1)$$

and the lattice parameters, magnetic, and electric vectors can be obtained by the following matrix:

$$\begin{pmatrix} 1/2 & 0 & -1/2 \\ -1/2 & 1/2 & 0 \\ 1 & 1 & 1 \end{pmatrix}. \quad (2)$$

Thus, by converting the structural data for the rhombohedral symmetry, the polarization magnitude per unit cell of the (0.6)$BiFeO_3$-(0.4)$PbTiO_3$ + 5 wt. % La sample was determined as 31.53(9) $\mu C/cm^2$. Besides, by using also the converted rhombohedral atomic positions, the centers of symmetry for cations (Bi^{3+}, Pb^{2+}, La^{3+}, Fe^{3+}, and Ti^{4+}) and anions (O^{2-}) were determined. After determining the effective electric charge, it was possible to obtain the polarization vector (**P**) and electric dipole moment per unit cell (P), which are listed in Table I. In hexagonal symmetry (Fig. 3(a)), the polarization vector points towards the 001_H direction, whereas in the rhombohedral symmetry (Fig. 3(b)), it points towards the 111_R direction. The magnetic moment vector points approximately to the 303_H (or 963_R) direction.

The average angles between magnetic and electric dipole moments ($\theta_{ME1} = 22.18(2)^\circ$ and $\theta_{ME2} = 157.81(8)^\circ$) are shown in Fig. 3(b), inset (i). The weak-ferromagnetism originating from the pure BF system cannot occur in the BFPT-5L compound, as stated in the Dzyaloshinskii and Morya prediction.[8,9] This is because the magnetization direction is not perpendicular to the 111_R direction in the rhombohedral symmetry of the BFPT-5L compound, as shown in Fig. 1(b). In fact, the intrinsic canted antiferromagnetic sublattice, which would lead to the weak-ferromagnetic order in BF compounds, is energetically favored only when magnetic moments are perpendicular to the 111_R direction.[43] Thus, the physical mechanism for the magnetoelectric coupling in BFPT-5L can be strongly affected by the magnetic arrangement shown in inset (i) of Fig. 3(b). Namely, the origin of the magnetoelectric coupling has been related to the quantum interaction between the induced polarization and current of spins, which originates from the noncollinear spin structure,[36,44] such as the one that occurs in the magnetic cycloid arrangement formed in the BF compound.[45] In this process, the coupling energy is zero when the polarization vector is perpendicular to the plane of magnetic moments, and it should reach its highest value when the vector is parallel to that plane.[36] Therefore, in our model, the magnetic moment lies within the *ac*-plane (in the hexagonal setting), whereas $\vec{\mu}$ is projected parallel ($\vec{\mu}\cos\theta_{ME1}$) and antiparallel ($\vec{\mu}\cos\theta_{ME2}$) to the $\vec{p}$ vector, generating an angle between magnetic and electric dipole moments. In this way, the coupling energy is still sufficient to generate a strong magnetoelectric coupling, as shown in Fig. 1(c). A complementary study was performed by modeling the electron density around the BFPT-5L cationic sites (Fig. 3(c)) in order to determine the influence of chemical bonds upon the ferroelectric, magnetic, and magnetoelectric properties. The three oxygen atoms (1, 2, and 3) form A-O bonds (R_1) that are stronger than any other formed in the perovskite cell, indicating covalent chemical bonds characterized by their high localized electron density (inset (ii) in Fig. 3(c)). In fact,

bonds A-A, B-A, and B-O are weaker and have a more ionic character, which explains why the structure becomes distorted in the [111] direction under cooling ($T < T_C$), undergoing a transition from cubic to rhombohedral symmetry. The strong R_1 bonds directly influence the ME coupling because they are responsible for the ferroelectric polarization (ferroelectric moment vector in the $[111]_R$ direction) and may also cause indirect influence because they distort the electronic orbitals, modifying the spin-orbit coupling and altering the magnetic and electronic configurations in the unit cells. Thus, these forces govern not only the ferroelectric direction (polarization vector direction) and the coupling angle (the angle between the magnetic and ferroelectric dipole moments), but the direction of the magnetic moment vector as well.

The physical implications for a multiferroic compound whose directions of magnetic and electric moments are neither perpendicular nor parallel (as in this case) can be assessed by investigating the magnetoelectric response. It is worth noting that the magnetoelectric coefficient shows a quadratic dependence ($\alpha_{33} \propto H^2$—see continuous line in Fig. 1(c)) with the magnetic field increasing to $H \sim 5$ kOe, where the magnetoelectric response tends to be saturated. This behavior clearly suggests a strain-mediated magnetoelectric coupling, originated from the intrinsic magnetostrictive response of the BFPT-5L compound.[13,14,46] In fact, in such a system, the configuration of magnetic and electric moments can be less energetic than one composed by exactly orthogonal/parallel ferroelectric and magnetic ordering vectors. This is because less time and energy are spent, under magnetic or electric fields, to reorient coupled ordering vectors in magnetoelectric systems with low coupling angles. These systems tend to present elevated magnetoelectric coefficients, as indeed shown for the BFPT-5L sample ($\alpha_{Max} \sim 3.5\,mV/cm \cdot Oe$—Fig. 1(c)). In fact, the ME effect is enhanced in BFPT-5L in comparison with other single-phased $BiFeO_3$-based compounds (for example, $\alpha_{33} \sim 0.4\,mV/cm \cdot Oe$ for $[Bi_{0.7}Sr_{0.3}]FeO_3$, $\alpha_{33} \sim 0.45\,mV/cm \cdot Oe$ for $[Bi_{0.7}Ba_{0.3}]FeO_3$, and $\alpha_{33} \sim 1.4\,mV/cm \cdot Oe$ for $[Bi_{0.7}\,Sr_{0.15}Ba_{0.15}]FeO_3$).[47] The potentialities for applying BFPT-L ceramics in magnetic sensing devices, by exploring their intrinsic magnetoelectric coupling, were recently pointed out.[46] Consequently, magnetoelectric devices composed by BFPT-5L should present a better performance due to their higher sensitivity and lower energy consumption, being suitable candidates for such technological applications.[46]

IV. CONCLUSIONS

Important features of the intrinsic magnetoelectric coupling mechanism in La modified $BiFeO_3$-$PbTiO_3$ solid solutions were pointed out by using high-resolution neutron and X-ray diffraction techniques, structural Rietveld refinement, and modeling of the electron density around cations. The magnetoelectric coupling angle is governed by covalent-like forces, which also affect the structural and ferroelectric distortions. The physical constraints beyond the magnetoelectric coupling angle are directly related to technological applications. Therefore, devices produced with materials that present low ME coupling angles, as those found for the BFPT-5L compound, should be faster, more sensitive, and more energy-efficient under the same operating conditions.

ACKNOWLEDGMENTS

The authors would like to thank the Brazilian agencies CNPq (proc. 305129/2010-4), FAPESP (proc. 2008/04025-0), Fundação Araucária de Apoio ao Desenvolvimento Científico e Tecnológico do Paraná (Prots. 22825, 24202 and 22870), and CAPES (PROCAD 082/2007) for financial support. V.F.F. also thanks CAPES for fellowship.

[1]A. J. Jacobson and B. E. F. Fender, J. Phys. C. **8**, 844 (1975).
[2]Y. N. Venevtsev *et al.*, Sov. Phys. Crystallogr. **5**, 594 (1960).
[3]W. M. Zhu and Z.-G. Ye, Ceram. Int. **30**, 1435 (2004).
[4]S. Dong, J.-F. Li, and D. J. Viehland, Mater. Sci. **41**, 97 (2006).
[5]J.-R. Cheng and L. E. Cross, J. Appl. Phys. **94**, 5188 (2003).
[6]T. Leist, T. Granzow, W. Jo, and J. Rodel, J. Appl. Phys. **108**, 014103 (2010).
[7]R. Palai, R. S. Katiyar, H. Schmid, P. Tissot, S. J. Clark, J. Robertson, S. A. T. Redfern, G. Catalan, and J. F. Scott, Phys. Rev. B **77**, 014110 (2008).
[8]T. Moriya, Phys. Rev. **120**, 91 (1960).
[9]I. Dzialoshinski, J. Phys. Chem. Solids **4**, 241 (1958).
[10]T. L. Burnett, T. P. Comyn, and A. J. Bell, J. Cryst. Growth **285**, 156 (2005).
[11]V. F. Freitas, I. A. Santos, E. R. Botero, B. M. Fraygola, D. Garcia, and J. A. Eiras, J. Am. Ceram. Soc. **94**, 754 (2011).
[12]N. A. Hill, J. Phys. Chem. B **104**, 6694 (2000).
[13]L. F. Cótica, F. R. Estrada, V. F. Freitas, G. S. Dias, I. A. Santos, J. A. Eiras, and D. Garcia, J. Appl. Phys. **111**, 114105 (2012).
[14]L. F. Cótica, V. F. Freitas, I. B. Catellani, I. A. Santos, D. Garcia, and J. A. Eiras, Appl. Phys. Lett. **101**, 172903 (2012).
[15]A. Singh, A. Gupta, and R. Chatterjee, Appl. Phys. Lett. **93**, 022902 (2008).
[16]M. A. Khan, T. P. Comyn, and A. J. Bell, IEEE Trans. Ultrason. Ferroelectr. Freq. Control **54**, 2583 (2007).
[17]T. P. Comyn, S. P. McBride, and A. J. Bell, Mater. Lett. **58**, 3844 (2004).
[18]V. F. Freitas, L. F. Cótica, I. A. Santos, D. Garcia, and J. A. Eiras, J. Eur. Ceram. Soc. **31**, 2965 (2011).
[19]C. B. R. Parente, V. L. Mazzocchi, J. Mestnik-Filho, Y. P. Mascarenhas, and R. Berliner, Nucl. Instrum. Methods Phys. Res. A **622**, 678 (2010).
[20]J. Rodriguez-Carvajal, Physica B **192**, 55 (1993).
[21]E. H. Kisi and C. J. Howard, *Applications of Neutron Powder Diffraction* (Oxford University Press, Oxford, 2008).
[22]F. Izumi and K. Momma, Solid State Phenom. **130**, 15 (2007).
[23]M. Yashima, N. Sirikanda, and T. J. Ishihara, J. Am. Chem. Soc. **132**, 2385 (2010).
[24]J.-P. Rivera, Eur. Phys. J. B **71**, 299 (2009).
[25]N. A. Spaldin and M. Fiebig, Science **309**, 391 (2005).
[26]W. Eerenstein, N. D. Mathur, and J. F. Scott, Nature **442**, 759 (2006).
[27]S. Bhattacharjee and D. Pandey, J. Appl. Phys. **107**, 124112 (2010).
[28]W.-M. Zhu, H.-Y. Guo, and Z.-G. Ye, Phys. Rev. B **78**, 014401 (2008).
[29]B. H. Toby, Powder Diffr. **21**, 67 (2006).
[30]J. B. Good Enough, *Magnetism and the Chemical Bond* (John Wiley & Sons, New York, 1963).
[31]H. A. Kramers, Physica **1**, 182 (1934).
[32]P. W. Anderson, Phys. Rev. **79**, 350 (1950).
[33]T. P. Comyn, T. Stevenson, M. A. Jawad, S. T. Turner, R. I. Smith, A. J. Bell, and R. Cywinski, J. Appl. Phys. **105**, 094108 (2009).
[34]T. P. Comyn, T. Stevenson, M. Al-Jawad, G. André, A. J. Bell, and R. Cywinski, J. Magn. Magn. Mater. **323**, 2533 (2011).
[35]R. Ranjan, V. Kothai, A. Senyshyn, and H. Boysen, J. Appl. Phys. **109**, 063522 (2011).
[36]D. Lebeugle, D. Colson, A. Forget, M. Viret, A. M. Bataille, and A. Gukasov, Phys. Rev. Lett. **100**, 227602 (2008).
[37]P. Fischer, M. PoIomska, I. Sosnowska, and M. Szymanskig, J. Phys. C **13**, 1931 (1980).
[38]I. Sosnowska, R. Przeniosto, P. Fischer, and V. A. Murashov, J. Magn. Magn. Mater. **160**, 384 (1996).

[39]I. Sosnowska, W. Schäfer, W. Kockelmann, K. H. Andersen, and I. O. Troyanchuk, Appl. Phys. A **74**, S1040 (2002).
[40]A. Palewicz, R. Przeniosło, I. Sosnowska, and A. W. Hewat, Acta Crystallogr., Sect. B: Struct. Sci. **63**, 537 (2007).
[41]A. G. Jackson, *Handbook of Crystallography for Electron Microscopists and Others* (Springer-Verlag Inc., New York, 1991).
[42]H. D. Megaw and C. N. W. Darlington, Acta Crystallogr. A **31**, 161 (1975).
[43]C. Ederer and N. A. Spaldin, Phys. Rev. B **71**, 060401 (2005).
[44]H. Katsura, N. Nagaosa, and A. V. Balatsky, Phys. Rev. Lett. **95**, 057205 (2005).
[45]I. Sosnowska, T. P. Neumaier, and E. Steichele, J. Phys. C **15**, 4835 (1982).
[46]D. Z. Montanher, V. F. Freitas, J. R. D. Pereira, L. F. Cótica, D. Garcia, J. A. Eiras, and I. A. Santos, J. Appl. Phys. **113**, 034102 (2013).
[47]V. B. Naik and R. Mahendiran, Solid. State Commun. **149**, 754 (2009).